International Association
Bridge Earthquake Engineering

The Third International Bridge Seismic Workshop, 3rd IBSW
Seattle, Washington, USA - October 1st to 4th, 2019

UNILATERAL CYCLIC LOADING TESTS ON REPAIRED 0.2-SCALE RC COLUMN MODELS USING SHCC

S. Yamamoto[(1)], K. Kinoshita[(2)], S. Lim[(3)] and K. Shinya[(4)]

[(1)] *Graduate School Doctoral Program Student, Mechanical and Civil Engineering Division, Gifu University, w3912013@edu.gifu-u.ac.jp*
[(2)] *Associate professor, Department of Civil Engineering, Gifu University, Kinosita@gifu-u.ac.jp*
[(3)] *Deros Japan Corporation, sclim@deros-japan.co.jp*
[(4)] *Toyo Matelan Corporation, shinyak@matelan.co.jp*

Abstract

Strain-hardening fiber-reinforced cement-based composites (SHCC) have the potential for enhancing the seismic performance of RC columns and repairing seismic damaged columns due to their strain-hardening and multiple fine cracks characteristics. Previous studies based on full-scale and small-scaled column models showed that use of SHCC could mitigate damage of cover and core concrete, local buckling of longitudinal bars. However, there is still uncertain for failure mechanism; local buckling, low cycle fatigue failure of longitudinal bars, damage of repaired cover and core concrete of SHCC repairing parts.

This study investigates failure mechanism of repaired RC columns using SHCC based on unilateral cyclic loading tests of 0.2-scaled RC column models that have been compared with a full-scaled RC column model with regarding to strength, ductility and so on in authors' previous studies in order to minimize the size effect of scaled column models. Following the authors' previous studies, this study repaired damaged 0.2-scaled RC columns which were tested in the authors' previous studies and carried out their cyclic loading tests. For repairing, this study used a spraying cement mortar with the 2 % volume of polyvinyl alcohol fiber having 40.0 μm diameter and 12 mm length after removing cover concrete of the damaged columns.

As a result of cyclic loading tests, the maximum strength of repaired models could recover to 90% degree. Horizontal flexure cracks were observed as multiple fine cracks to the maximum strength and the SHCC of cover concrete area mitigated the spalling and local buckling of longitudinal bars. As results of observation of the repair part with X-ray CT system and SEM, cracks occurred from longitudinal bars propagated to the circumferential direction at the boundary of spraying cement mortar layers. It is said that the decreasing of the cross section of the column due to the crack propagation leads to sudden strength drop after the maximum strength. In addition, the fracture process of longitudinal bars was clarified by observing dimples on fracture surface.

Keywords: Scaled RC column; Cyclic loading test; Repair performance; SHCC; Failure mechanism

1. Introduction

Although concrete materials are generally used as one of structural materials, the tensile strength performance is inferior to the compressive strength clearly. For example, the tensile strength is one-tenth of the compressive strength and concrete materials show brittle behavior under tensile stress loading. Recently, fiber reinforced cement composites that mixed short fiber to improve the tensile strength performance have been developed. The specific behavior of especially strain-hardening fiber-reinforced cement-based composites (SHCC) that mixed polyvinyl alcohol (PVA) fibers have been investigated [1, 2]. SHCC have the potential for enhancing the seismic performance of RC columns and seismic repair of damaged columns due to their strain-hardening and multiple fine cracks characteristics. Previous studies based on full-scale and small-scale reinforced concrete (RC) column models showed that use of FRC such as SHCC could mitigate damage of cover and core concrete, local buckling of longitudinal bars [3-5]. However, there is still uncertain for failure mechanism; local buckling and low cycle fatigue failure of longitudinal bars and damage of repaired cover and core concrete of SHCC repairing area.

Meanwhile, small-scaled models are generally used to investigate dynamic behavior of RC structures and members experimentally. However, the behavior of a small-scaled model can't agree well with that of a full-scaled model due to the scale ratio of a small-scaled model. It is hard to reflect results of small-scaled models in a design because of the size effect, which the dynamic performance decreases so that the size of a model is big. For this reason, the use of a small-scaled model which the size effect is minimized as much as possible, is desirable in an experiment of RC structures.

This study investigates failure mechanism of repaired RC column using SHCC based on unilateral cyclic loading tests of 0.2-scaled RC column models that have been compared with a full-scaled RC column model [6] with regarding to strength, ductility and so on in authors' previous study [7] in order to minimize the size effect of scaled column models. In addition, damaged parts in the tests were observed with X-ray CT system and scanning electron microscope (SEM) to clarify the failure mechanism.

This paper begins with a brief overview of the RC column models, SHCC and repair method. From results of unilateral cyclic loading tests, repair performance and damaged parts are shown. Finally, this paper summarized failure mechanism based on the observation of damaged parts with X-ray CT system and SEM.

2. RC Column Models and Repair Method

2.1 RC column models

Figure 1 shows the shape and size of RC column models. The height of the column model is 1350 mm and the radius of circle cross-section is 400 mm. In this study, models were 0.2-scale of the full-scale column [6]. Two column models are denoted as D10 model and D13 model. In D10 model, deformed 10 mm diameter 16 longitudinal bars were set at every 71 mm interval (Figure 1 (a)). In D13 model, deformed 13 mm diameter 10 longitudinal bars were set at every 114 mm interval (Figure 1 (b)). The longitudinal reinforcement ratio was 1.0 % in each models. Round 3 mm diameter bars were used for ties and set at every 65 mm interval. Based on the tensile tests of the deformed bars, yield strength of the longitudinal bars of D10, D13 and ties were 351, 320 and 360 N/mm^2, respectively. Table 1 shows models list in this study. Damaged models by first cyclic loading tests [7] were repaired to clarify the failure mechanism at the repaird parts. D10-150 and D13-150 models [8] were repaired by using SHCC and were denoted as D10-150-1R and D13-150-1R models. D10-60 and D13-60 models [9] were repaired by using SHCC and bars to be damaged at the upper repair parts were denoted as D10-150-2R and D13-60-2R models. After the repair, second cyclic loading tests were performed. D10-150-2R and D13-60-2R models which were damaged by second cyclic loading tests were repaired and were denoted as D10-150-3R and D13-60-3R models. After the repair, third cyclic loading tests were performed. Figure 2 shows damaged models by first cyclic loading tests. D10-150 model was damaged in the area of 130 mm by 200 mm (Figure 2 (a)). D13-150 model was damaged in the area of 65 mm by 150 mm (Figure 2 (b)). D10-60 model was damaged in the area of 150 mm by 300 mm (Figure 2 (c)). D13-60 model was damaged in the area of 200 mm by 250 mm (Figure 2 (d)).

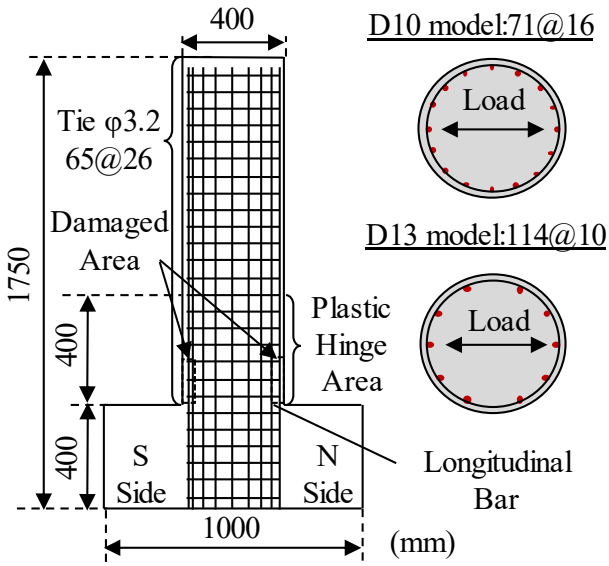

Figure 1. Shape and size of models

Table 1. Models list in this study

Loading	Models			
First[6]	D10-150[7]	D13-150[7]	D10-60[8]	D13-60[8]
	Damage			
	Buckling	Spalling	Buckling	Buckling
Second	Repair Materials (First Repair)			
	SHCC	SHCC	SHCC+Bars	SHCC+Bars
	Repaired Models			
	D10-150-1R	D13-150-1R	D10-150-2R	D13-60-2R
	Damage			
	Fracture	Buckling	Buckling	Buckling
Third	Repair Materials (Second Repair)			
	-	-	SHCC+Bars	SHCC+Bars
	Repaired Models			
	-	-	D10-150-3R	D13-60-3R
	Damage			
	-	-	Fracture	Fracture

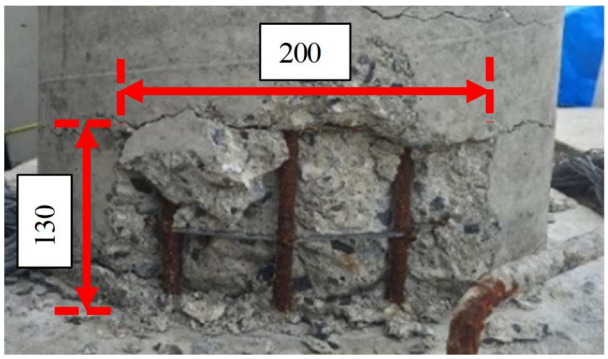

(a) D10-150 model (N side) [7]

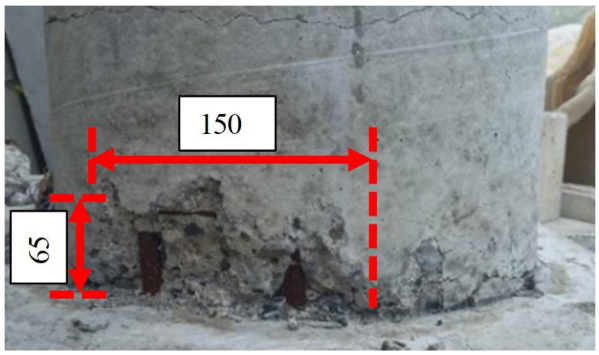

(b) D13-150 model (N side) [7]

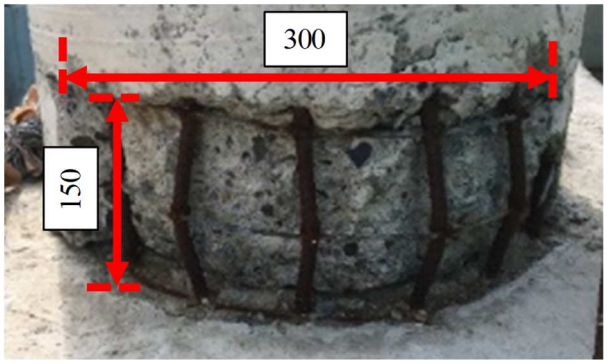

(c) D10-60 model (N side) [8]

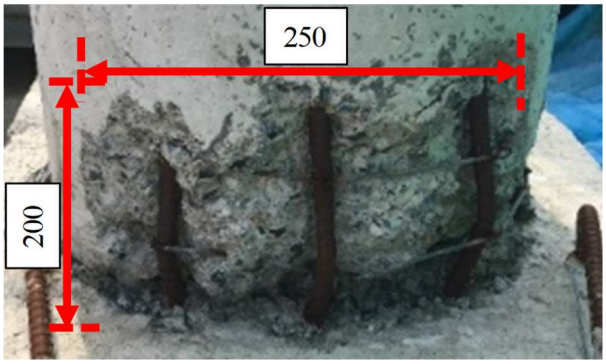

(d) D13-60 model (N side) [8]

Figure 2. Damaged models by first cyclic loading tests[6]

2.2 Repair method (1R)

Figure 3 and Figure 4 shows the repair area and the chipped area of the 1R models. The cover concrete of the damaged models chipped from the base to the height of 300 mm. The chipped depth was the thick of cover concrete including longitudinal bars diameter. In the D10-150-1R model, the depth of the chipping was 28 mm and one tie was broken. In the D13-150-1R model, the depth of the chipping was 35 mm and three ties were

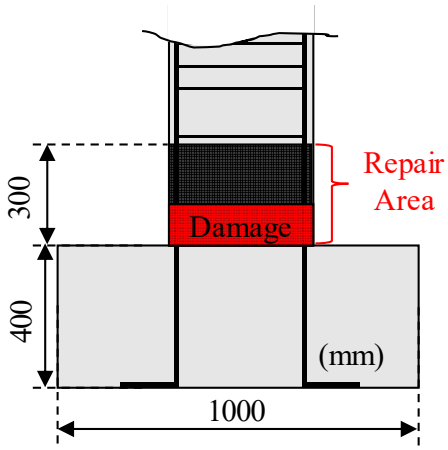

Figure 3. Repair area (1R)

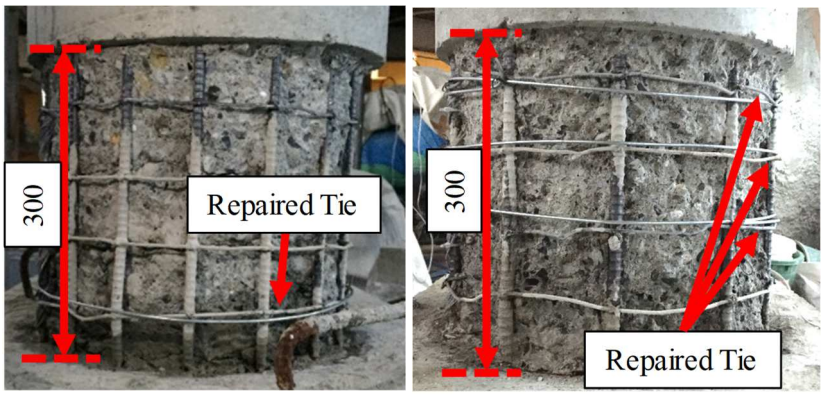

(a) D10-150-1R **(b) D13-150-1R**

Figure 4. Chipped area (N side)

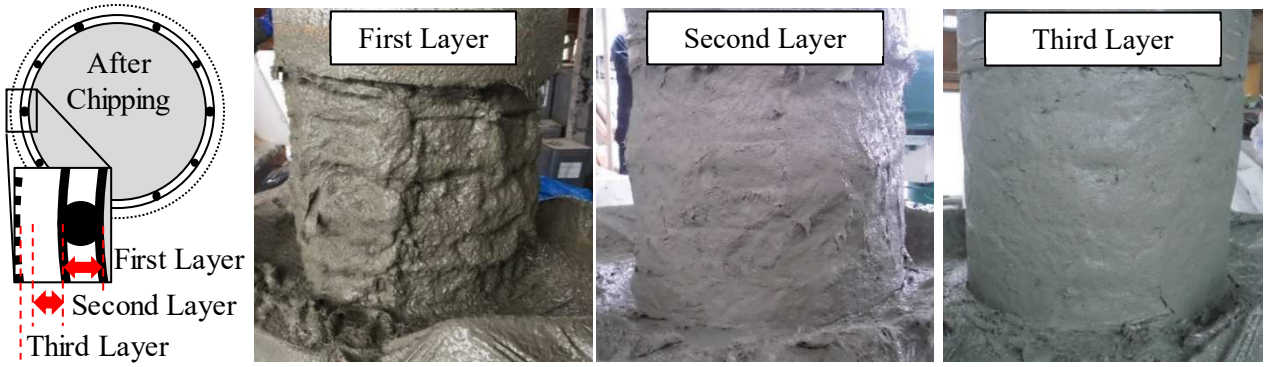

Figure 5. Spraying SHCC (1R)

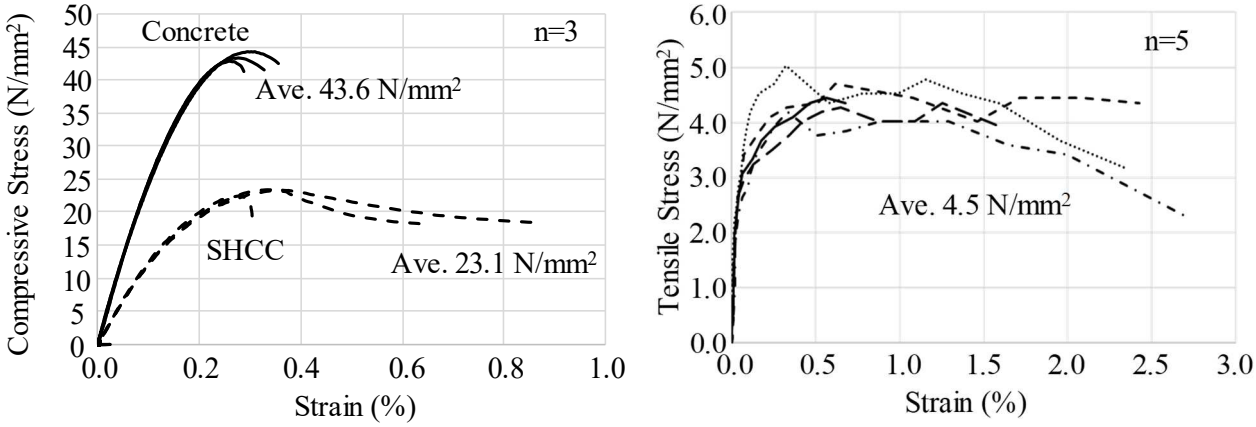

(a) Compressive **(b) Tensile**

Figure 6. Material strength (1R)

broken. The broken ties was repaired by using new same tie. Buckling longitudinal bars were not repaired. Figure 5 shows the method of the spraying SHCC. The SHCC was sprayed dividing into 3 layers. First layer was sprayed at the area of longitudinal bars. Second layer was sprayed at the area of cover concrete. Third layer was sprayed as finishing. The SHCC was a cement mortar with the 2 % volume of polyvinyl alcohol (PVA) fiber having 40.0 μm diameter and 12 mm length. Water-binder ratio and unit water amount was 40 %, 335 kg/m^3. Figure 6 shows SHCC strength based on cylinder tests. Cylinders tests performed at 14 days curing. The average of compressive strength was 23.1 N/mm^2. On the other hand, the average of tensile strength was 4.5 N/mm^2.

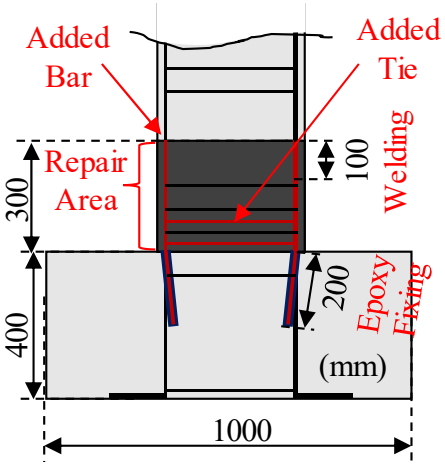

Figure 7. Repair area (2R)

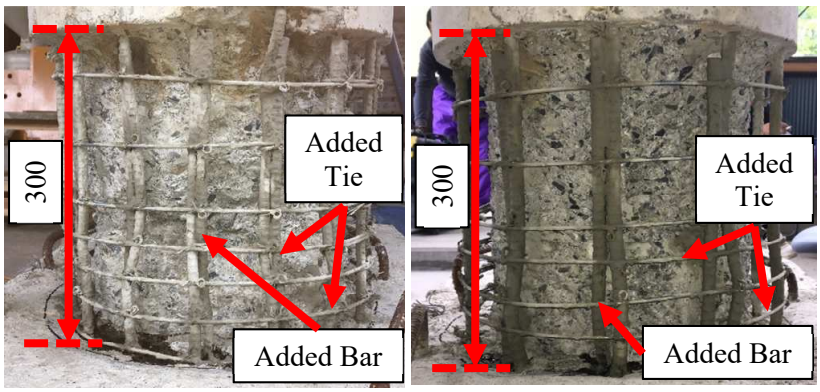

(a) D10-150-2R **(b) D13-60-2R**

Figure 8. Chipped area (N side)

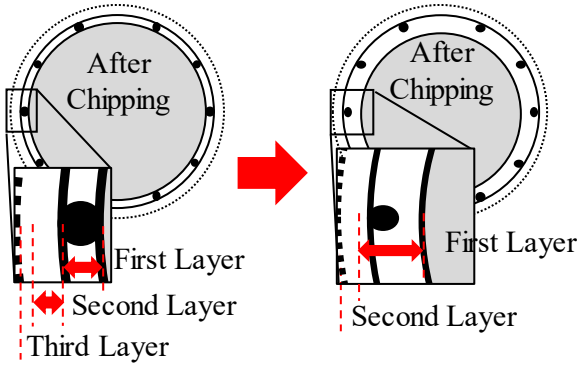

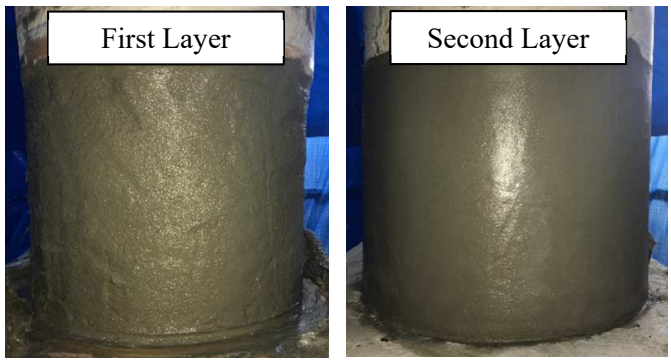

Figure 9. Spraying SHCC (2R)

2.3 Repair method (2R)

Figure 7 and Figure 8 shows the repair area and the chipped area of the 2R models. In 2R models, additional bars were inserted and method of the spraying were improved to be damaged at the upper repair part. The cover concrete of the damaged models chipped from the base to the height of 300 mm. The chipped depth was around 30 mm from the longitudinal bars back. Inserted additional bars were fixed by welding and epoxy resin. Figure 9 shows the method of the spraying SHCC. The SHCC was sprayed dividing into 2 layers. First layer was sprayed from longitudinal bars back to the area of the cover concrete. Second layer was sprayed as finishing.

2.4 Repair method (3R)

Figure 10 and Figure 11 shows the repair area and the chipped area of the 3R models. In 3R models, additional bars and ties were inserted at the area of the fracture of longitudinal bars. Method of the spraying was same as 2R models. The cover concrete of the damaged models chipped from the base to the height of 600 mm. The chipped depth was around 30 mm from the longitudinal bars back. Inserted additional bars were fixed by welding. Figure 12 shows SHCC strength based on cylinder tests. Cylinders tests performed at 14 days curing. The average of compressive strength was 36.7 N/mm^2. On the other hand, the average of tensile strength was 3.9 N/mm^2.

3. Unilateral Cyclic Loading Tests

Figure 13 shows experiment set-up of models. The 0.2-scaled model was fixed at hooting and two jacks were used for lateral cyclic loading and axial loading. The upper part of the specimen is a concrete block to attach two jacks and united the specimen. The axial loading jack was movable to lateral direction due to fixing at the

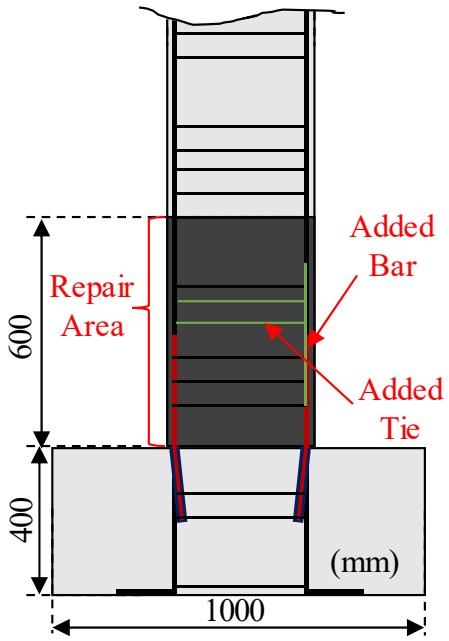

Figure 10. Repair area (3R)

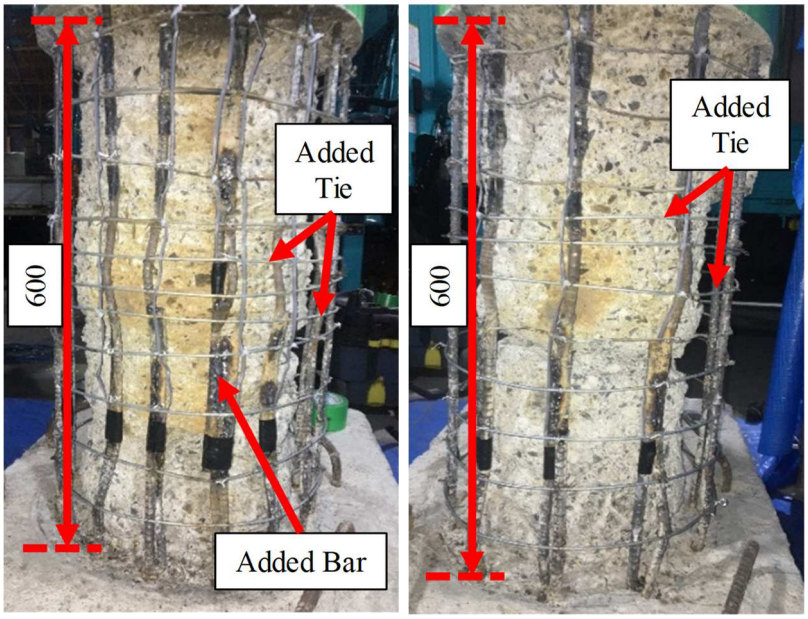

(a) D10-150-3R **(b) D13-60-3R**

Figure 11. Chipped area (N side)

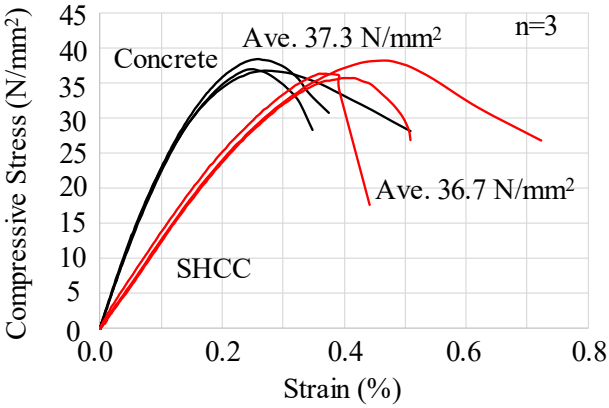

(a) Compressive

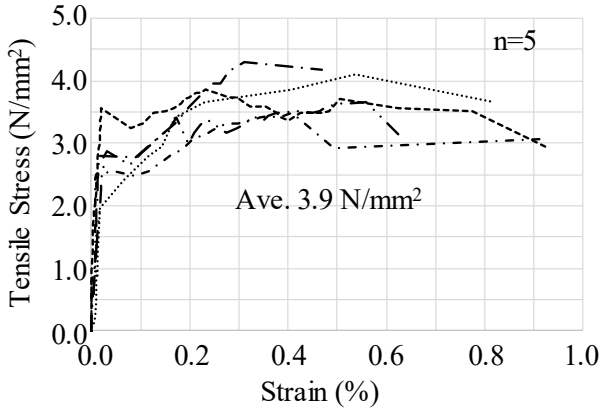

(b) Tensile

Figure 12. Material strength (3R)

linear slider. Figure 14 shows loading sequence. Yield displacement (δ_y) was the same value in authors' previous study [7,8]. A loading-controlled testing was conducted until yield displacement. After the yield displacement, a displacement-controlled testing on the lateral direction with an axial load was conducted.

4. Test Results

Figure 15 shows hysteresis curves of D10-150-1R model and D13-150-1R model. In the D10-150-1R model (δ_y=4.44 mm, P_y=32.3 kN), horizontal cracks and multiple fine cracks were observed before ±3.0 δ_y (δ=13.3 mm). The maximum strength reached 62.5 kN at ±3.5 δ_y (δ=15.5 mm). After the maximum strength, the strength gradually decreased. Break of the tie was observed at 5.5 δ_y (δ=24.4 mm). Break of the longitudinal bar was observed at -13.0 δ_y (δ=57.7 mm). The cyclic loading test finished at ±16.0 δ_y (δ=71.0 mm) because the strength reached 50% strength of the maximum strength. In the D13-150-1R model (δ_y=3.89 mm, P_y=35.8 kN), the maximum strength reached 64.0 kN at ±5.5 δy (δ=21.4 mm). After the maximum strength, the strength gradually decreased. Break of the tie was observed at +10.0 δy (δ=38.9 mm). The cyclic loading test finished at ±18.0 δy (δ=70.2 mm) because the strength reached 50 % strength of the maximum strength. 1R models

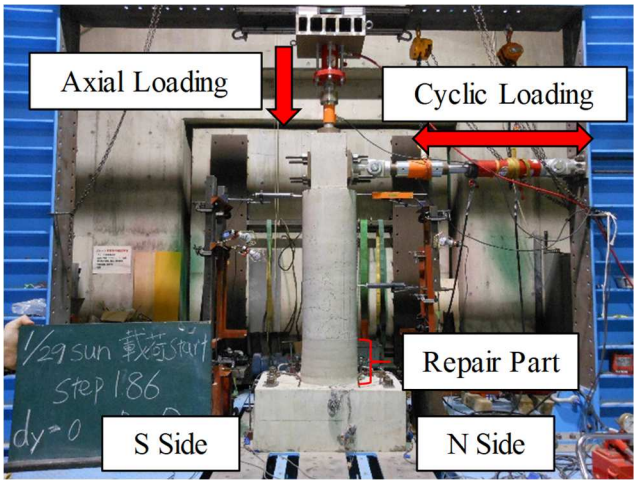

Figure 13. Test set up

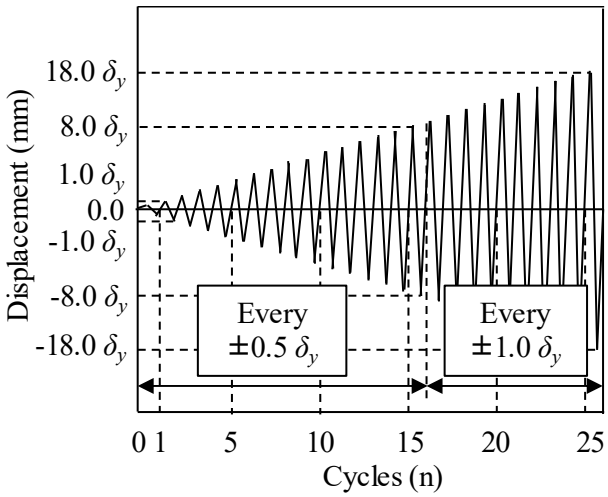

Figure 14. Loading sequence

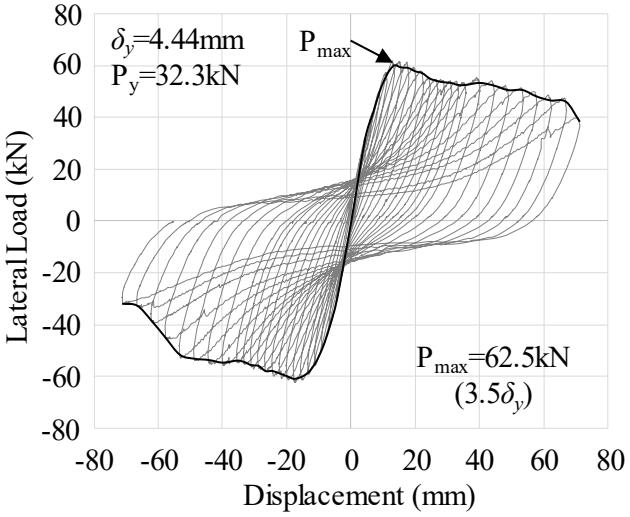

(a) D10-150-1R

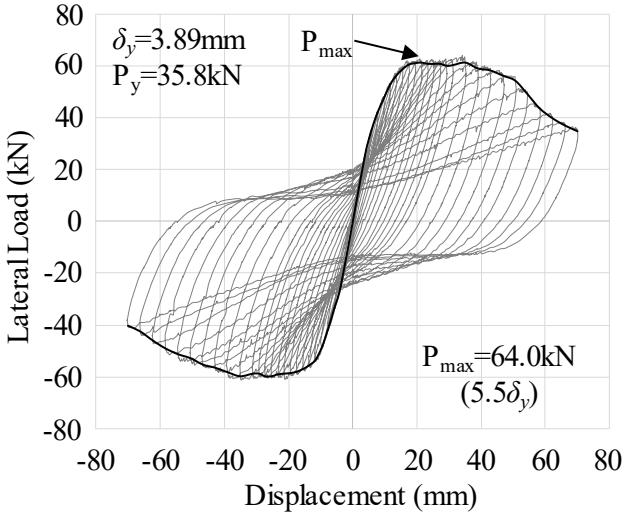

(b) D13-150-1R

Figure 15. Hysteresis curves (1R)

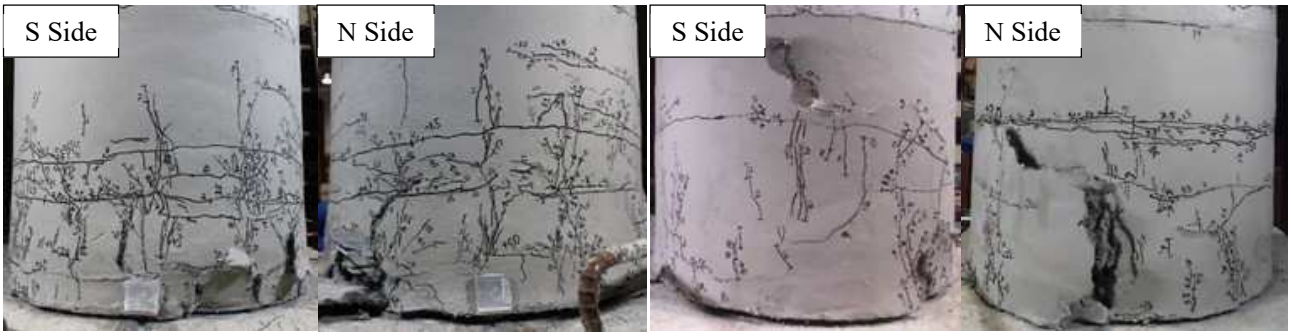

(a) D10-150-1R **(b) D13-150-1R**

Figure 16. Damaged models by second cyclic loading tests

were a flexure failure mode. Figure 16 shows the damaged 1R models by second cyclic loading tests. Flexure lateral cracks were observed as multiple fine cracks at the face of repair material. The spalling of repair material was not observed in D10-150-1R model. On the other hands, the spalling of repair materials of the D13-150-1R model was the larger area than that of D10-150-1R model and propageted to the circumferential direction.

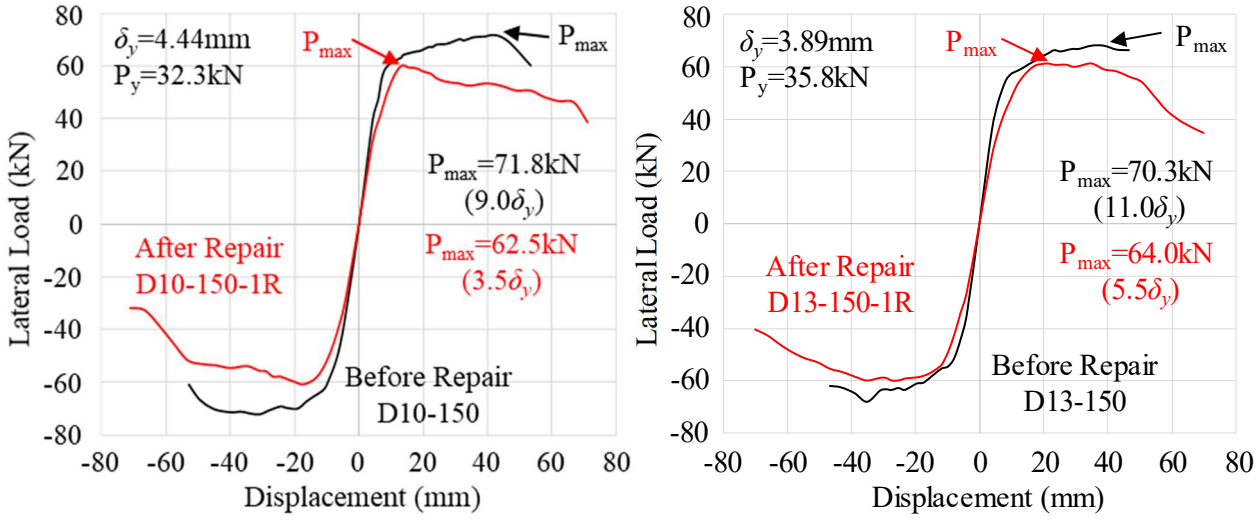

(a) D10 model **(b) D13 model**

Figure 17. Envelope curves of the before and after repair

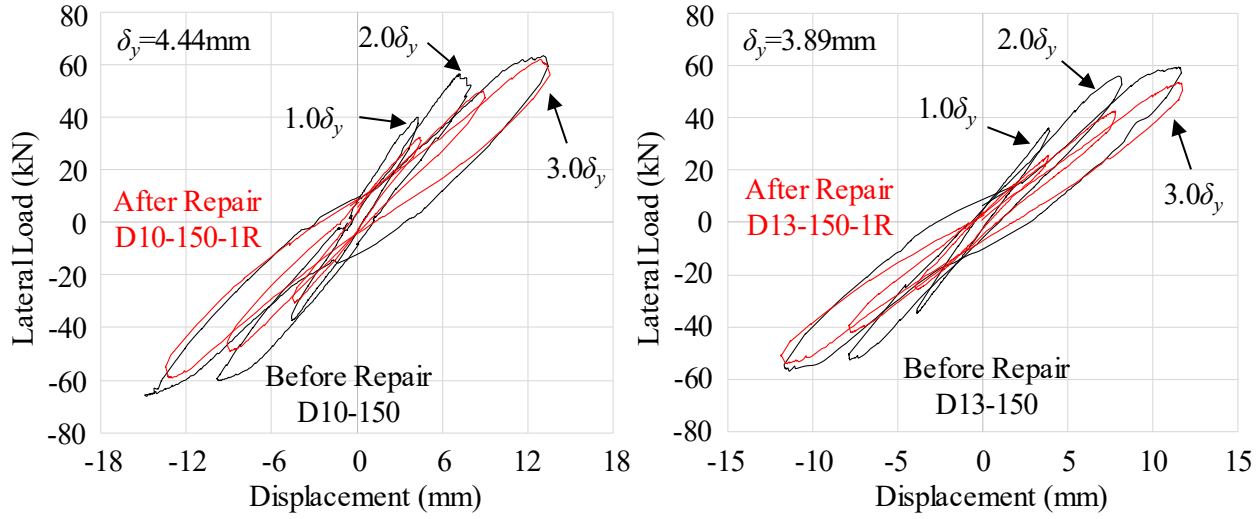

(a) D10 model **(b) D13 model**

Figure 18. Hysteresis lopes in the 1.0 δ_y, 2.0 δ_y and 3.0 δ_y

Figure 17 shows envelope curves of the before and after repair models. Although the initial stiffness of after repair models was smaller than that of before repair models, the maximum strength of the after repair models recovered to 90 % degree of the maximum strength of the before repair models. The discrepancy of the initial stiffness was due to the difference of the pull-out displaccement. The maximum strength of the D10-150-1R model gradually decreased after the maximum strength due to the buckling of longitudinal bars by first cyclic loading tests. Figure 18 shows hysteresis lopes of before and after repair models in the ±1.0 δ_y, ±2.0 δ_y and ±3.0 δ_y. The stiffness of before repair models gradually dropped from ±1.0 δ_y to ±3.0 δ_y. On the other hands, the stiffness of after repair models did not drop as before repair models. It is considered that the discrepancy of the stiffness drop was due to the difference of the pull-out displaccement. The pull-out displaccement of after repair models were larger than that of the before repair models. Therefore, it is said that the deformation of after repair models were smaller than that of before repair models.

Figure 19 shows envelope curves of all models. The initial stiffness and maximum strength of 2R models were recovered due to the improvement of spraying and inserting longitudinal bars. The ductility of the 2R models

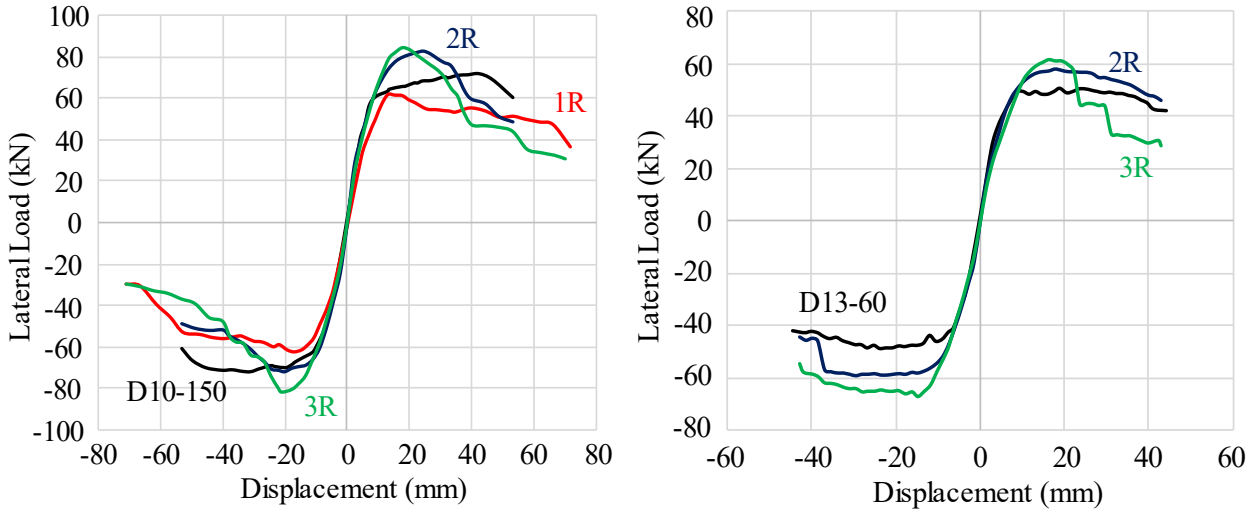

(a) D10 Model **(b) D13 Model**

Figure 19. Envelope curves of all models

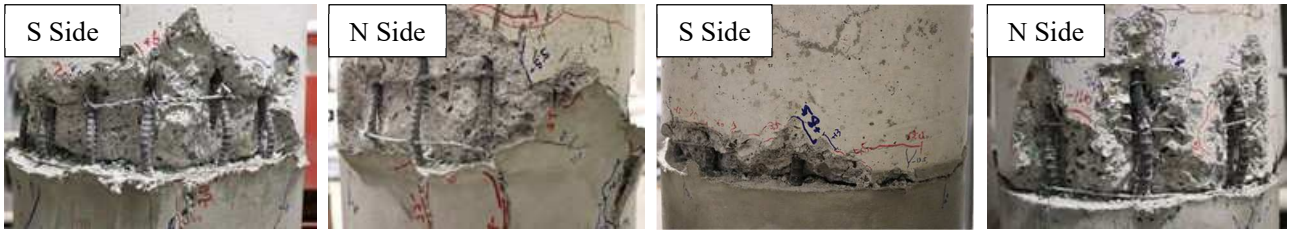

(a) D10-150-2R **(b) D13-60-2R**

Figure 20. Damaged models by second cyclic loading tests

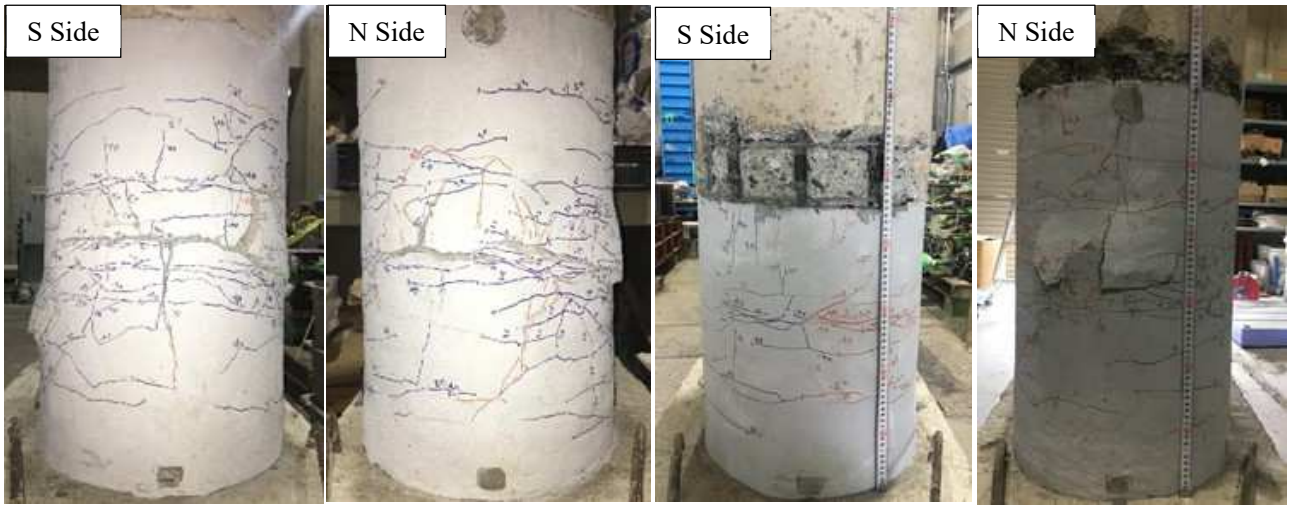

(a) D10-150-3R **(b) D13-60-3R**

Figure 21. Damaged models by third cyclic loading tests

were small because flexure failure could be occured at the upper repair part. Figure 20 shows damaged models by second cyclic loading tests. Flexure failure could be occured at the upper repair part and the damage of the repair part was slight. The initial stiffness, maximum strength and ductility of 3R models were the almost same as 2R models. After the maximum strength of D13-60-3R model, the strength were sudden dropped due to the buckling of longitudinal bars at the S side of D13-60-3R model. Figure 21 shows damaged models by third

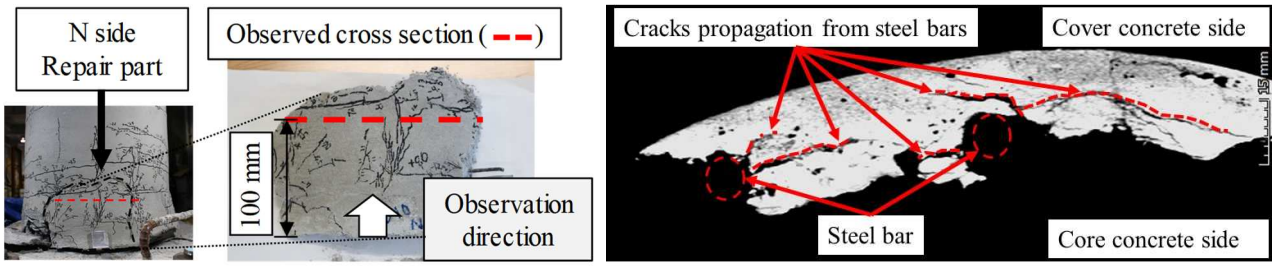

(a) Observation point **(b) Result of observation by X-ray CT**

Figure 22. Results of observation of the repaired part (1R)

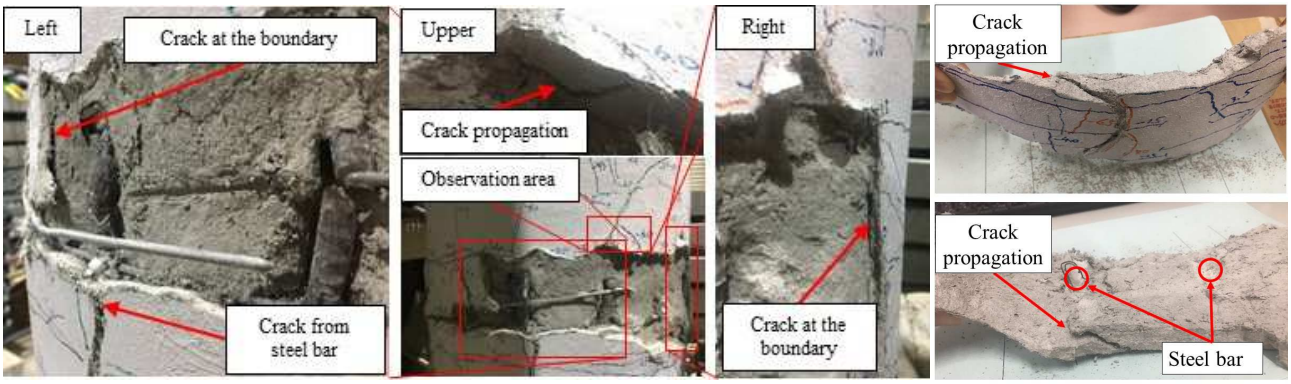

Figure 23. Results of observation of the repaired part (2R)

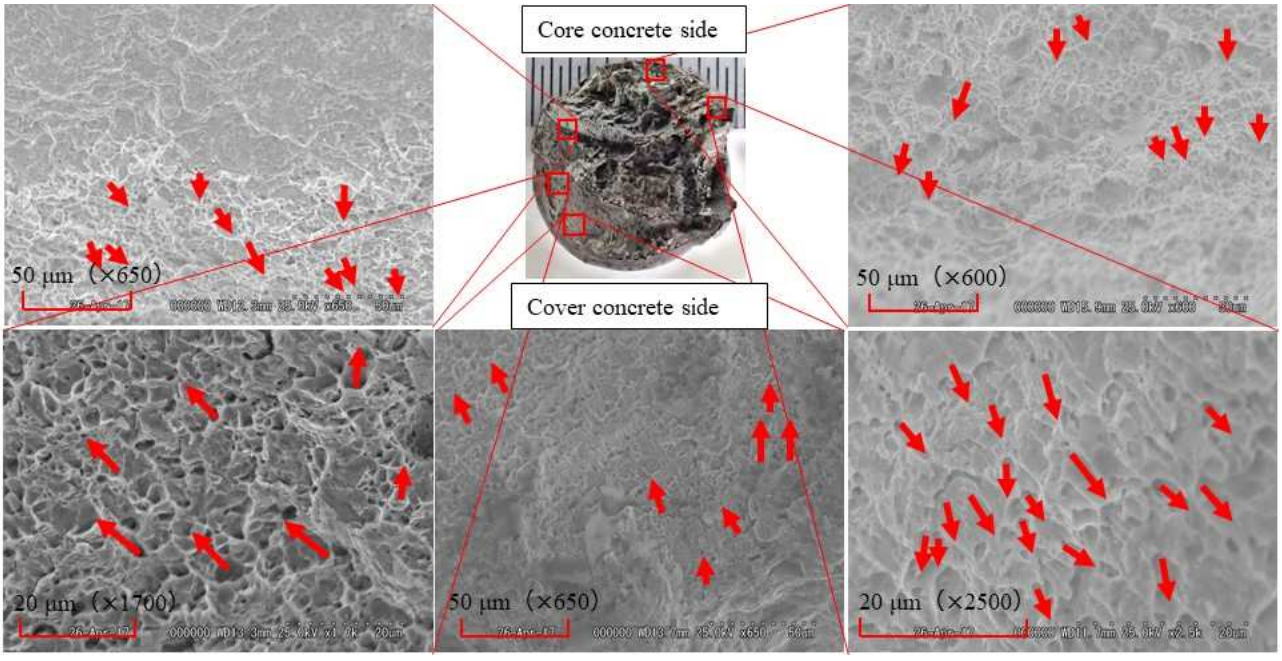

Figure 24. Results of observation of the fractured surface

cyclic loading tests. The damage of the area inserted additional bars was slight. The damaged area of 3R models was same as that 2R models.

5. Observations of Damgage Parts

5.1 Observation of repair part with X-ray CT system

The repaire part was observed with X-ray CT system to clarify the failure mechanism. This X-ray CT system is non-destructive testing machine that makes the cross section images by irradiating X-ray in a subject. Figure 22 shows results of observation of the repair part of the D10-150-1R model. Observation point in repair part was at the N side of D10-150-1R model. Observation direction was a height direction from the hooting surface. Figure 22 (b) shows results of observation of the cross section at 100 mm in height from the hooting surface. The upper part of the cross section is the outermost edge of the column and the lower part of the cross section is the core concrete side. Cracks propagated from steel bar and these cracks did not propagate to the outermost edge of the column and propagated to the circumferential direction. In addition, the cracks that propagated from the steel bar next to each other were united. It is said that the damage that was different from the crack distribution of the outside of the cover concrete was observed in the inside of the column. The propagated path of the cracks, which propagated to the circumferential direction, agree well with the position of layers in spraying SHCC because the spraying SHCC was divided in each layer. Furthermore, this crack propagation is caused by spalling in the repair part and decreased the cross section of the column. Therefore, it is concluded that the decreasing of the cross section of the column due to the crack propagation leads to the strength drop after the maximum moment strength of the D10-150-1R model.

Figure 23 shows results of observation of the repair part of the D10-150-3R model. Observation point in repair part was the area from 300 mm to 450 mm in height at the N side of D10-150-3R model. The spalling of the repair material started from longitudinal bars and occurred in a range among vertical crack along longitudinal bars and flexure lateral cracks which were formed in multiple fine cracks. In the left side of the observation area, cracks at the boundary of the spraying and from the longitudinal bar were observed. In the upper side of the observation area, the crack propagation from the longitudinal steel bar was observed. In the right side of the observation area, the crack at the boundary of the spraying was observed. Results of observation of spalling flakes showed that the cracks from longitudinal bars propagated to the circumferential direction.

5.2 Observation of the fracture surface of the longitudinal bar with SEM

As a study by Takiguti et al. [10], it is considered that the fracture of the longitudinal steel bar is caused by a fatigue failure for low cycle after the maximum strength. In this study, the fracture surface of the longitudinal bar were observed with the scanning electron microscope (SEM) in order to clarify the fracture process. Figure 24 shows the results of observation of the fracture surface of the longitudinal bar of outermost edge in the N side of the D10-150-1R model. The upper side of fracture surface showed the core concrete side and the lower side showed the cover concrete side. In the core concrete side, the rough fracture surface and the dull luster were observed. On the other hands, in the cover concrete side, the flat fracture surface and the metallic luster were observed. In addition, in the middle area of the fracture surface, the torn fracture surface were observed. It is assumed that the longitudinal bar was fractured by propagating of cracks under the cyclic loading. The fracture surface of core concrete side was the area where tension and compression was loaded under the cyclic loading. Therefore, it is said that the fatigue crack was propagated in the core concrete side. The cross-section of the longitudinal bar was decreased due to the fatigue crack propagation. The tensile crack was propagated in the cover concrete side. The crack propagation were showed by observing with SEM. Dimples, which can be observed in the ductile fracture surface [11, 12, 13], were observed. It is said that the fracture process of the longitudinal bar was clarified because the direction of dimples shows the direction of the crack propagation.

6. Conclusions

This study investigated failure mechanism of repaired RC column using SHCC based on unilateral cyclic loading tests of 0.2-scaled RC column models. The conclusions of this study described as follows.

1. The maximum strength of the repaired model could recover to 90 % degree. Horizontal flexure cracks were observed as multiple fine cracks to the maximum strength and the SHCC of cover concrete area mitigated the spalling and local buckling of longitudinal bars.

2. As a result of observation of the repaired part, cracks occurred from longitudinal bars propagated to the circumferential direction at the boundary of spraying cement mortar layers. In addition, the fracture process of longitudinal bars was clarified by observing dimples on fracture surface.
3. Therefore, the decreasing of the cross section of the column due to the crack propagation leads to sudden strength drop after the maximum strength. The improvement of the ductility may be shown by mitigating the crack propagation after maximum strength.

7. Acknowledgements

Special thanks to Professor Yuichi Uchida and Professor Minoru Kunieda of Gifu University for valuable comments and suggestions in the cyclic loading tests. Thanks to members of this research group at Gifu University, Mr. Yoshitomo Yano and Mr. Masamune Takahashi for conducting the cyclic loading tests.

8. References

[1] K. Rokugo, Y. Uchida, M. Moriyama and S. Lim (2007): Direct tensile behavior and size effect of strain-hardening fiber-reinforced cement-based composites (SHCC). *6th International conference on fracture mechanics of concrete and concrete structures*, 3, 1429-1434.

[2] P. Jun and V. Mechtcherine (2010): Behavior of Strain-hardening Cement-based Composites (SHCC) under monotonic and cyclic tensile loading, Part 1- Experimental investigations. *Journal of Cement and Concrete Composites*, Vol.32, 801-809.

[3] H. Shimizu, K. Kosa, H. Goda and A. Ogawa (2011): Study of seismic reinforcement with area of high performance cement jacket, *Japan Society of Civil Engineers*, *Journal of structural engineering*, Vol.57A, 405-417.

[4] R. G. Zafra, K. Kawashima, T. Sasaki, K. Kajiwara and M. Nakayama (2012): Effect of Polypropylene Fiber Reinforced Cement Composites for Enhancing the Seismic Performance of a Full-Scale Bridge Column Based on E-defense Excitation, *15th World conference on earthquake engineering*, Lisbon, Portugal.

[5] W. Zhang, H. Matsuzaki and K. Kawashima (2013): Effect of Tie Bar Volume on the Seismic Performance of Polypropylene Fiber Reinforced Columns based on Hybrid Loading Experiments, *Journal of Japan Society of Civil Engineers*, A1, Vol.69, No.4, I_807-I_820.

[6] S. Iwata, M. Seki, T. Uezuki and H Achiha (2011): Damage degree comparison of full-scaled model and the 0.5-scaled model of the RC circular column by the loading experiment, Collection of Japan Society of Civil Engineering, 66th Annual Assembly, I-383, pp. 765-766. (in Japanese)

[7] S. Yamamoto and K. Kinoshita (2018): Developing of a Small-scaled RC Column Model Reproducing a Full-scaled RC Column, 7th Asia Conference on Earthquake Engineering, Bangkok, Thailand.

[8] K. Kinoshita and S. Yamamoto (2017): Effects of longitudinal steel bars size on hysteresis of small-scale RC column model, Proceedings of the Japan Concrete Institute, Vol.39, No.2, 673-678. (In Japanese)

[9] S. Yamamoto and K. Kinoshita (2017): Experimental consideration about size effect of the cyclic loading performance of the circular RC pier, Proceedings of the Japan Concrete Institute, Vol.39, No.2, 667-672. (In Japanese)

[10] M. Takiguchi, T. Ikenaga, T. Kitahara and Y. Kajita (2017): Sectional average strain amplitude distribution in bar area between ribs for low-cycle fatigue failure estimation due to buckling of rebar, *Japan Society of Civil Engineers*, *Journal of structural engineering*, Vol.63A, 834-846. (In Japanese)

[11] S. Fujiki (2002): A viewpoint of the fatigue failure and the fractured surface of the machine part, The Nikkan Kogyo Shinbun, LTD. (In Japanese)

[12] G. F. Pittinato, V.Kerlins, A. Phillips and M. A. Russo (1975); SEM/TEM fractography handbook. Metals and Ceramics Information Center.

[13] Y. Shioya, Y. Matsuo, T. Hattori and H. Kawada (2010); Fractography-Analysis and Case Studies. Tekuno System Corporation. (In Japanese)